Neuro-Oncology

25(4), 735–747, 2022 | https://doi.org/10.1093/neuonc/noac199 | Advance Access date 17 August 2022

BH3 mimetics targeting BCL-XL impact the senescent compartment of pilocytic astrocytoma

Florian Selt, Romain Sigaud, Gintvile Valinciute, Philipp Sievers, Julia Zaman, Clara Alcon, Simone Schmid, Heike Peterziel, Jessica W. Tsai, Romain Guiho, Juan Pedro Martínez-Barbera, Stefan Pusch, Jing Deng, Yifan Zhai, Cornelis M. van Tilburg, Martin U. Schuhman, Ahmed El Damaty, Pratiti Bandopadhayay, Christel Herold-Mende, Andreas von Deimling, Stefan M. Pfister, Joan Montero, David Capper, Ina Oehme, Felix Sahm, David T.W. Jones, Olaf Witt, and Till Milde

Hopp Children's Cancer Center Heidelberg (KiTZ), Heidelberg, Germany (F.S., R.S., G.V., H.P., C.v.T., S.M.P., I.O., F.Sa., D.T.W.J., O.W., T.M.); Clinical Cooperation Unit Pediatric Oncology, German Cancer Research Center (DKFZ) and German Consortium for Translational Cancer Research (DKTK), Heidelberg, Germany (F.S., R.S., G.V., H.P., C.v.T., I.O., O.W., T.M.); KiTZ Clinical Trial Unit (ZIPO), Department of Pediatric Hematology, Oncology, Immunology and Pulmonology, Heidelberg University Hospital, Heidelberg, Germany (F.S., C.v.T., S.M.P., O.W., T.M.); Department of Neuropathology, Institute of Pathology, Heidelberg University Hospital, Heidelberg, Germany (P.S., J.Z., S.P., A.v.D.; F.Sa.); Clinical Cooperation Unit Neuropathology, German Consortium for Translational Cancer Research (DKTK), German Cancer Research Center (DKFZ), Heidelberg, Germany (P.S., J.Z., S.P., A.v.D., F.Sa.); Institute for Bioengineering of Catalonia (IBEC), Barcelona Institute of Science and Technology (BIST), 08028, Barcelona, Spain (C.A., J.M.); Charité-Universitaetsmedizin Berlin, Corporate Member of Freie Universitaet Berlin, Humboldt-Universitaet zu Berlin, and Berlin Institute of Health, Department of Neuropathology, Berlin, Germany (S.S., D.C.); German Cancer Consortium (DKTK), German Cancer Research Center (DKFZ), Partner Site Berlin, Berlin, Germany (S.S., D.C.); Dana-Farber/Boston Children's Cancer and Blood Disorder Center, Boston, Massachusetts, USA (J.W.T., P.B.); Developmental Biology and Cancer Research & Teaching Department, Birth Defects Research Centre, Great Ormond Street Institute of Child Health, University College London, London, UK (R.G., J.P.M.B.); Ascentage Pharma (Suzhou) Co, Ltd, Suzhou, Jiangsu Province, China (J.D., Y.Z.); Department of Neurosurgery, University Hospital Tübingen, Tübingen, Germany (M.U.S.); Pediatric Neurosurgery Division, Department of Neurosurgery, Heidelberg University Hospital, Heidelberg, Germany (A.E.D.); Broad Institute of MIT and Harvard, Cambridge, Massachusetts, USA (P.B.); Department of Pediatrics, Harvard Medical School, Boston, Massachusetts, USA (P.B.); Department of Neurosurgery, Heidelberg University Hospital, Heidelberg, Germany (C.H.M.); Division of Pediatric Neurooncology, German Cancer Research Center (DKFZ) and German Consortium for Translational Cancer Research (DKTK), Heidelberg, Germany (S.M.P.); Division of Pediatric Glioma Research, German Cancer Research Center (DKFZ), Heidelberg, Germany (D.T.W.J.)

Corresponding Author: Till Milde, MD, MHBA, Hopp Children's Cancer Center Heidelberg (KiTZ), Im Neuenheimer Feld 430, 69120, Heidelberg, Germany (t.milde@kitz-heidelberg.de).

Abstract

Background. Pilocytic astrocytoma (PA) is the most common pediatric brain tumor and a mitogen-activated protein kinase (MAPK)-driven disease. Oncogenic MAPK-signaling drives the majority of cells into oncogene-induced senescence (OIS). While OIS induces resistance to antiproliferative therapies, it represents a potential vulnerability exploitable by senolytic agents.

Methods. We established new patient-derived PA cell lines that preserve molecular features of the primary tumors and can be studied in OIS and proliferation depending on expression or repression of the SV40 large T antigen. We determined expression of anti-apoptotic BCL-2 members in these models and primary PA. Dependence of senescent PA cells on anti-apoptotic BCL-2 members was investigated using a comprehensive set of BH3 mimetics.

Results. Senescent PA cells upregulate BCL-XL upon senescence induction and show dependency on BCL-XL for survival. BH3 mimetics with high affinity for BCL-XL (BCL-XLi) reduce metabolic activity and induce mitochondrial apoptosis in senescent PA cells at nano-molar concentrations. In contrast, BH3 mimetics without BCL-XLi activity, conventional chemotherapy, and MEK inhibitors show no effect.
Conclusions. Our data demonstrate that BCL-XL is critical for survival of senescent PA tumor cells and provides proof-of-principle for the use of clinically available BCL-XL-dependent senolytics.

Key Points

- New patient-derived PA models for studies in oncogene-induced senescence and proliferation.
- BH3 mimetics targeting BCL-XL induce apoptosis in senescent PA cells.
- BCL-XL is the first reported target for senolytic treatment of PA.

Importance of the Study

PAs are the most common pediatric brain tumors. Incompletely resected tumors frequently progress after cessation of anti-proliferative treatments. Relapses and multiple lines of salvage-therapy cause substantial long-term morbidity and toxicity. Because most PA cells are in OIS, they are not sensitive to anti-proliferative treatments and can therefore serve as source for relapse and progression. OIS may, thus, be an unexploited vulnerability of PA cells targetable by senolytic drugs. We here report the first evidence supporting the use of BCL-XLi to target the so far un-targeted senescent compartment of PA. Senolysis induced by clinically available BCL-XLi could open a new avenue to improve long-term outcomes of PA patients. Based on the data presented, conceptualization of a clinical trial investigating BCL-XLi in relapsed and progressive PAs is currently being discussed.

Pilocytic astrocytomas (PA) are the most frequent pediatric brain tumors and the largest subgroup of pediatric low-grade gliomas (pLGG).[1] In contrast to the excellent 10-year overall survival of over 90%, the event-free survival of pLGG patients is only ca. 50%.[2] More than half of the incompletely resected patients treated with conventional chemotherapy progress and require one or more lines of salvage therapy.[2] PAs are characterized by activation of the mitogen-activated protein kinase (MAPK) pathway.[3,4] Although the mitogen-activated protein kinase (MEK) inhibitors (MEKi) selumetinib and trametinib were shown to be well tolerated and effective in progressive or relapsing pLGGs in phase I/II clinical trials and retrospective case studies,[5–10] tumors may relapse or progress shortly after discontinuation of treatment.[5,8,9] Therefore, development of complementary new treatment strategies is needed to improve long-term outcome of PA patients.

MAPK pathway activation leads to oncogene-induced senescence (OIS) in PA.[11] Less than 5% of primary PA cells express the proliferation marker Ki67,[12] indicating that the majority of cells is not cycling. While cells in OIS are not responsive to anti-proliferative treatments and may constitute a reservoir of tumor cells that can lead to tumor relapse upon cessation of anti-proliferative therapies,[13] OIS might represent a yet unexploited complementary vulnerability of PA targetable by senolytic drugs.

In 2015, Zhu et al. identified the activation of pro-survival networks in senescent cells and silenced expression of the key nodes of these networks to target senescent cells.[14] Subsequently, pharmacological clearance of senescent cells by compounds of mechanistically diverse classes including BH3 mimetics was described.[14–17] BH3 mimetics are inhibitors of the anti-apoptotic B-cell lymphoma 2 (BCL-2) family members,[15–18] which comprise BCL-2, BCL-XL, Bcl-2-like protein 2 (BCL-W), induced myeloid leukemia cell differentiation protein (MCL-1) and BCL2 related protein A1 (BFL-1). Within the tightly balanced process of intrinsic apoptosis, the main function of these anti-apoptotic BCL-2 members is to prevent the induction of mitochondrial membrane potential breakdown and apoptosis.[19]

Previous data from our group indicated the senolytic activity of the BH3 mimetic navitoclax, an inhibitor of BCL-2, BCL-XL, and BCL-W, in PA.[20] The lack of more PA models, that would allow for validation and comprehensive testing of senolytic compounds in OIS, is a major obstacle. While short-term cultures can only be incompletely characterized and do not yield enough material for comprehensive studies, the few existing long-term pLGG-derived in vitro models (BT40,[21] JHH-NF1-PA1,[22] Res186, Res259[23]) are not suited for testing in senescence because they continuously proliferate and do not recapitulate the PA senescence biology.

The aim of the present study was to evaluate the senolytic properties of BH3 mimetics in PA and to decipher their translational potential. We made use of our PA cell line DKFZ-BT66[24] and a set of three completely newly established PA cell lines suitable for testing in proliferation and OIS depending on expression or repression of SV40 large T antigen. The aim was to identify the BCL-2 members essential for survival of senescent PA cells, which need to be targeted by BH3 mimetics to induce senolysis.

Materials and Methods

Processing of Primary Patient Samples

Primary PA tumor material (DKFZ-BT308, DKFZ-BT314, and DKFZ-BT317) was collected during therapeutic intervention. Informed consent for sample collection and use was obtained within the study S-304/2014, which was approved by the institutional review board of the University of Heidelberg. Clinical, histopathological, and molecular data of the samples are summarized in Supplementary Table 1. For processing and culture of primary samples, see Supplementary Methods.

Inducible Expression of Simian Vacuolating Virus 40 Large T Antigen (SV40-TAg)

For generation of pCW57.1 GFP-TAg, allowing for doxycycline-inducible co-expression of destabilized GFP (dsGFP) and SV40-TAg, see Supplementary Methods. Primary PA cell cultures were transduced after 2 to 7 days in culture with 3 ml pCW57.1 GFP-TAg supernatant in 6-well plates (Corning). ABM medium and 1 μg/ml doxycycline were added 6 h after infection. Work with lentiviruses was approved by the authorities (internal project number 80935) and performed in a biosafety level two laboratory.

Cell Culture and Drugs

DKFZ-BT66, DKFZ-BT308, DKFZ-BT314, and DKFZ-BT317 cell lines were grown as described before.[24] For details, see Supplementary Methods.

Metabolic Activity, DSS Calculation, and Drug Combination Profiling

For measurement of metabolic activity see Supplementary Methods. Drug sensitivity scores were calculated based on dose–response data using the R package DSS (v 1.2).[25] DSS3 mode was used, with output ranging from 0 (insensitive) to 100 (highly sensitive).

Cell Viability Assessment and Cell Counting

Five days prior to treatment 0.8×10^6 cells/well were seeded in 6-well plates (Corning) without doxycycline. Medium changes were performed every second to third day. Cells were then incubated with different BH3 mimetics at concentrations indicated or DMSO. After 72 h, the remaining attached cells were collected and cell number as well as viability were assessed using trypan-blue based automated cell counting (Vi-CELL XR automated cell counter; Beckmann Coulter).

Senescence-associated β-Galactosidase Staining

Senescence-associated (SA) β-galactosidase staining was performed as described.[24] 1×10^5 cells were seeded per well of a 6-well plate (Corning) 5 days prior to fixation without doxycycline. Images were taken with a Nikon Eclipse Ts2 microscope and Nikon Elements software (v 5.20).

Gene Expression Analysis

Gene expression analysis of PA cell lines was performed using Human Genome U133 Plus 2.0 chips (Affymetrix GeneChips®) with $n = 3$ independent biological replicates per condition. Affymetrix U133 Plus 2.0 expression array data of primary PA and normal cerebella was from R2 (Tumor Pilocytic astrocytoma (DKFZ) - Kool; R2 internal identifier: ps_mkheidel_mkdkfz209_u133p2). Array data was MAS5.0 normalized. Gene expression data of cell lines were downloaded from GDSC database (GDSC2).[26] Gene set enrichment analysis (GSEA) was done using GSEA software (v 4.1.0).[27,28] Single sample GSEA (ssGSEA)[29] was performed using the public server of GenePattern (www.genepattern.org).[30] BCL2 and BCL2L1 expression was analyzed in previously published single cell RNA sequencing data of primary PA.[31]

Western Blot and Immunoprecipitation

For information about antibodies used see Supplementary Methods. Western blot analysis was performed as described before.[24] Immunoprecipitation (IP) was done using Dynabeads™ Protein G Immunoprecipitation Kit (Invitrogen, 10007D) following the manufacturer's instructions. Antibodies were crosslinked to Dynabeads™ using freshly dissolved 20 mM dimethyl-pimelimidate (DMP) in 0.2 M triethanolamine buffer.

Tissue Micro Array and Immunohistochemical Staining

A tissue micro array of 83 PAs (CNS WHO grade I), part of the LOGGIC Core study, was generated and stained, for details, see Supplementary Methods. Inconspicuous CNS tissue adjacent to low-grade gliomas was used as normal controls ($n = 16$).

shRNA Mediated Gene Silencing

The lentiviral vector pGIPZ (Horizon Discovery Biosciences Limited) was used for shRNA knockdowns of BCL-XL. A mix of four shRNAs with the following

clone IDs (all from Horizon Discovery Biosciences Limited) and mature antisense sequences were used: V3LHS_641297 (GCATCTCCTTGTCTACGCT); V3LHS_413478 (AAATTCTAGAAAACTAGCT); V2LHS_269487 (TTTCCGACTGAAGAGTGAG); V3LHS_393128 (CACTAAACTGACTCCAGCT). For details on lentivirus production and infection, see Supplementary Methods. Protein samples for determination of knockdown efficiency were harvested 96 h after transduction. The amount of remaining attached cells was counted 14 days after transduction using Vi-CELL XR automated cell counter (Beckmann Coulter).

Real Time Quantitative Reverse Transcription Real-time PCR (RTqPCR)

RNA extraction, cDNA synthesis, and RTqPCR were performed as described before.[24] For information about primers used, see Supplementary Methods.

Gene Panel Sequencing and DNA Methylation Analysis

Capture-based next-generation DNA sequencing was performed on a NextSeq 500 instrument (Illumina) and DNA methylation analysis done as described.[32,33] For details, see Supplementary Methods.

Droplet Digital PCR (ddPCR)

All ddPCR experiments were conducted on the QX200 Droplet Digital PCR System (Bio-Rad) and analysis was performed using QuantaSoft Analysis Pro software (Bio-Rad), for details, see Supplementary Methods.

BH3 Profiling and Caspase-3 Activity

BH3 profiling experiments were performed as described before,[34] for details as well as on caspase-3 activity measurement see Supplementary Methods.

Measurement of Mitochondrial Membrane Potential (MMP)

Loss of MMP was measured using a tetramethyl rhodamine ethylester (TMRE) mitochondrial membrane potential assay kit (Cayman chemicals, Item No. 701310) following the manufacturer's instructions. For details see Supplementary Methods.

Data Availability and Statistics

Data were generated by the authors and are available on request. For details on statistics see Supplementary Methods.

Results

Establishment of New Patient-derived PA In Vitro Models

Short-term cultures from native tissue of three fresh PA tumors (Supplementary Table 1) were transduced with pCW57.1 GFP-TAg, allowing for doxycycline inducible expression of SV40-TAg to circumvent OIS. Culture of transduced primary cells in the presence of doxycycline allowed for establishment of long-term cell lines (>15 passages). DNA-methylation patterns, established for molecular classification of brain tumors,[33] revealed a stable methylome of all patient-derived cell lines at passage 7 and 15 clustering close to the DNA-methylation group of the corresponding primary samples (Figure 1A). Copy number plots (CNPs) derived from these DNA-methylation analyses were flat as expected for PA (Supplementary Figure. 1A).[35] CNPs indicated the presence of a BRAF-fusion in DKFZ-BT308 and DKFZ-BT317 (Supplementary Figure 1A) confirmed by ddPCR and RTqPCR on DNA and mRNA level (Supplementary Figure 1B–E). Gene panel sequencing detected a *BRAF V600E* mutation in DKFZ-BT314 (Supplementary Table 2), confirmed by ddPCR (Supplementary Figure 1F). ddPCR experiments indicated a nearly 100% tumor cell purity of all new models (Supplementary Figure 1B, C and F) explaining the close proximity but distinct difference from primary PA bulk tumors (containing also microenvironmental cells) on DNA-methylation level (Figure 1A).

The MAPK Pathway Activity Score (MPAS)[36] (Figure 1B) as well as phosphorylation status of ERK1/2 (Thr202/Tyr204) (Supplementary Figure 1 G) revealed activation of the MAPK-pathway in all cell lines. Robust proliferation of the new cell lines was observed only in the presence of doxycycline (proliferation; +DOX), and withdrawal of doxycycline (OIS; –DOX) led to growth arrest in all cell lines (Figure 1C) following repression of SV40 TAg (Figure 1D). All PA cell lines showed expression of the senescence marker $p21^{Cip1}$ on protein level (Figure 1E) and marked SA-beta-galactosidase positivity (Supplementary Figure 1H) in OIS mode. Gene expression analysis revealed upregulation of gene sets known to be upregulated in senescence (BUHL SASP,[20] FRIDMAN SENESCENCE UP,[37] and BT66 OIS UP[24]) and downregulation of gene sets known to be downregulated in senescence (BT66 OIS DOWN[24]) in all three new cell lines in the absence of doxycycline (Figure 1E). In summary, we established three new patient-derived PA cell lines that preserved molecular characteristics of their primary tumors and that are uniquely suitable for drug studies in OIS conditionally induced by repression of SV40-TAg after expansion.

BH3 Mimetics with High Binding Affinity for BCL-XL Preferentially Decrease Metabolic Activity of PA Cells in Oncogene-Induced Senescence

Navitoclax, a BH3 mimetic targeting BCL-2, BCL-XL, and BCL-W, decreased metabolic activity of DKFZ-BT66,

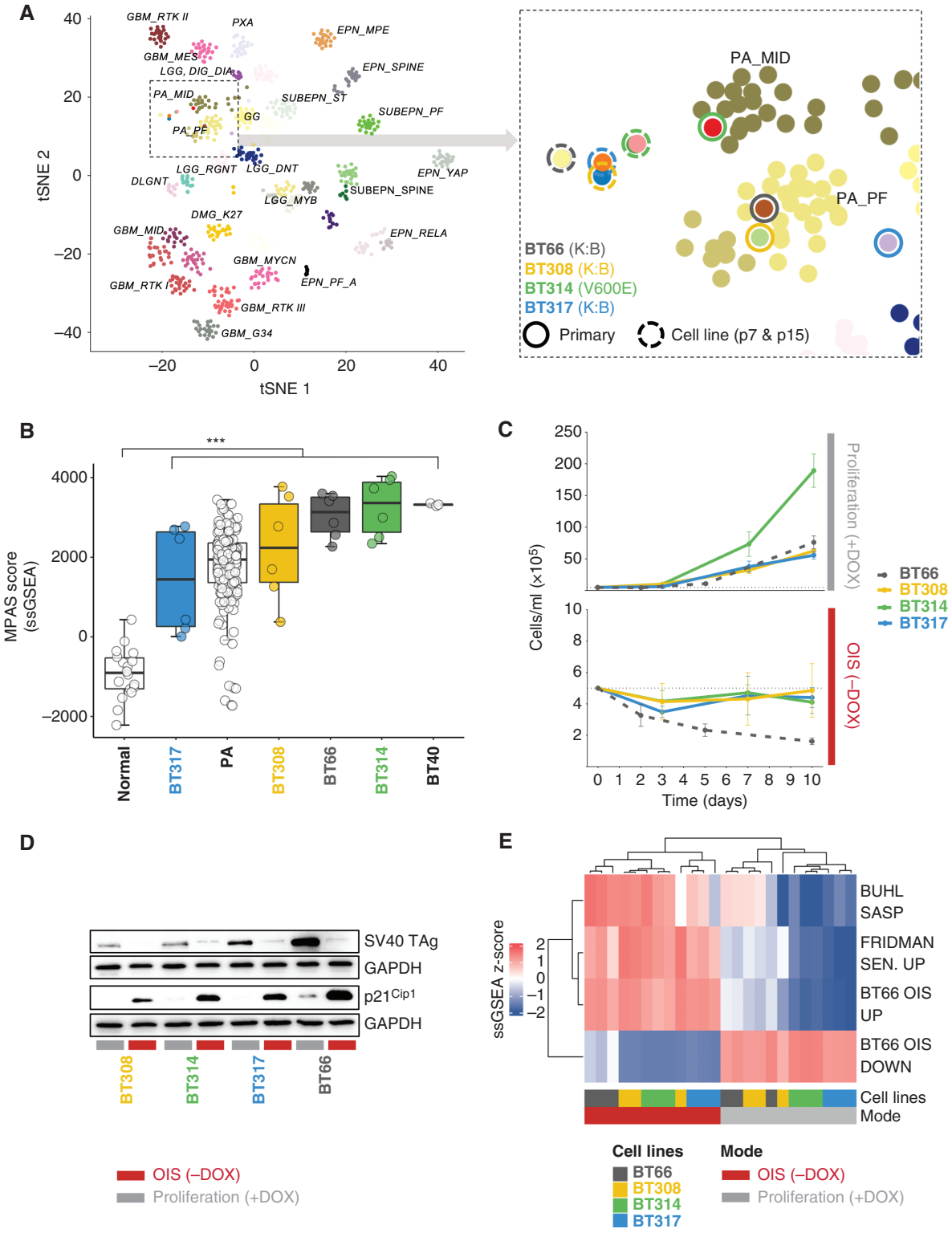

Fig. 1 Characterization of new patient-derived PA in vitro models DKFZ-BT308, DKFZ-BT314, and DKFZ-BT317. (A) t-SNE analysis of DNA methylation profiles of pediatric brain tumors (selected tumor types from mnp V12.3 reference set; www.molecularneuropathology.org), midline PA (PA_MID) and posterior fossa PA (PA_PF) enlarged on the right. Dashed circles: PA cell lines from p7 and p15 (passage 7 and 15), closed circles: corresponding primary samples. (B) MPAS signature ssGSEA scores. normal: normal cerebellum; PA: primary PA. ***Tukey multiple comparisons of means adjusted *P*-value: 2.7×10^{-6}. Expression data: ps_mkheidel_mkdkfz209_u133p2. (C) Cell counts of PA cell lines in proliferation or OIS. DOX: doxycycline; DKFZ-BT66: historical data. (D) Western blot of SV40 TAg and $p21^{Cip1}$. OIS: 5 days of doxycycline (DOX) withdrawal. (E) ssGSEA z-scores of senescence gene sets. $N = 3$ independent expression samples per condition. DOX: doxycycline.

–BT314, and –BT317 at nano-molar concentrations, validating the preferential susceptibility in OIS previously described in DKFZ-BT66[20] in two more models (Figure 2A). DKFZ-BT308 was relatively resistant to navitoclax in OIS and proliferation.

To identify the precise inhibitory profile needed for the induction of senolysis in PA, we tested a comprehensive set of BH3 mimetics with different inhibitory profiles (Table 1), compared to chemotherapeutics and MEKi (Figure 2B). Vincristine and vinblastine showed high DSS[25] (indicating high sensitivity) only in proliferation (DSS > 30 for all cell lines) but not in OIS (DSS = 0), as expected. The DSS for venetoclax, a BCL-2 selective inhibitor, MCL-1 inhibitors (A-1210477, S63645, AZD5991), and MEKis (trametinib, selumetinib, binimetinib) were overall low (<7), independent of OIS and proliferation. In contrast, the DSS for all inhibitors with strong affinity to BCL-XL indicated sensitivity of DKFZ-BT66, –BT314, and –BT317 in OIS (DSS > 33). IC_{50} values in OIS for all tested BCL-XLi were in the nanomolar range (Figure 2C) and the cell lines were among the most navitoclax-sensitive compared to 751 cell lines from the GDSC2 database (ranks: DKFZ-BT66:10/755; DKFZ-BT314: 39/755; DKFZ-BT317: 43/755) (Supplementary Figure 2A). DKFZ-BT308 was relatively resistant to all BCL-XLi, in OIS and proliferation. The differential DSS (dDSS; DSS^{OIS} minus $DSS^{proliferation}$) for all BCL-XLi were positive in the BCL-XLi sensitive cell lines, indicating a preferential susceptibility in senescence and a senolytic mechanism of action (Figure 2D). No positive dDSS was observed for BH3 mimetics without BCL-XL affinity or MEK-inhibitors. The dDSS of vinca alkaloids were negative, indicating sensitivity only in proliferation. The IC_{50}s of the BCL-XLi navitoclax, A-1331852, and A-1155463 were at least 8.5-fold higher in nonneoplastic brain-derived control NHA TAg cells compared to the BCL-XLi sensitive PA cell lines (Figure 2E and Supplementary Figure 2B). Taken together, we identified senolytic activity of BCL-XLi on metabolic activity level in senescent PA cell line models.

BCL-XL is Expressed in Primary PA, PA Tumor Cell Lines, and Upregulated in Oncogene-induced Senescence

Following the observation of exclusive sensitivity to BCL-XLi in the responsive PA cell lines, we investigated the expression of anti-apoptotic BCL-2 members in PA with a specific focus on BCL-XL. Expression of *BCL2L1* (encoding BCL-XL) mRNA (Figure 3A) and abundance of BCL-XL protein were confirmed in primary PA samples (Figure 3B and C; Supplementary Table 3). Of note, *BCL2L1* mRNA expression was significantly higher in normal CNS tissue but BCL-XL protein was significantly higher expressed in PA. The four PA cell lines expressed *BCL2L1*/BCL-XL and showed upregulation in OIS compared to proliferation (Figure 3D and E). Upregulation in OIS was not detected for the remaining anti-apoptotic Bcl-2 members BCL-2, BCL-W, and MCL-1 (Supplementary Figure 3A and B). *BCL2* transcription was significantly lower in the PA cell lines compared to bulk PA and no BCL-2 protein was detected by Western blot in the PA cell lines, consistent with the observation that BCL-2, in contrast to BCL-XL, is predominantly expressed in the tumor infiltrating immune cells (Supplementary Figure 3C). In summary, we confirmed BCL-XL target expression in primary PA and cell lines, and showed upregulation of BCL-XL in senescence in PA cell lines.

BCL-XL Inhibition Reduces Viable Cell Number and Induces Mitochondrial Apoptosis in Senescent PA Cells

Navitoclax treatment led to displacement of anti-apoptotic BCL-XL from pro-apoptotic BAK in all PA cell lines demonstrating target engagement (Figure 4A). The BCL-XLi A-1331852 and navitoclax significantly reduced the viable cell numbers at a concentration of 40 nM and higher in DKFZ-BT314 and –BT317 (Figure 4B). In contrast, the BCL-2 inhibitor venetoclax and the MCL-1 inhibitor S63845 did not significantly impact the number of viable cells in DKFZ-BT314 and only to a limited extent in DKFZ-BT317 (Figure 4B). This observation was in line with the respective metabolic activity data: metabolic activity IC_{50}s for venetoclax and S63845 were >3 µM in both models. A-1331852 and navitoclax led to a significant loss of MMP in the senescent PA cell lines DKFZ-BT314 and DKFZ-BT317 (Figure 4C) and an activation of caspase-3 (Figure 4D) indicating induction of mitochondrial apoptosis. Caspase 3 activation upon navitoclax treatment was significantly lower in proliferating DKFZ-BT314 and DKFZ-BT317 indicating a preferential induction of apoptosis in senescent PA cells (Supplementary Figure 4A). Taken together, this data confirmed the on-target effect and an in-class effect of BCL-XLi on viable cell number, mediated by mitochondrial apoptosis in senescent PA cells.

Senescent PA Cell Lines Depend on BCL-XL to Maintain Viability and to Prevent Mitochondrial Outer Membrane Permeabilization (MOMP)

DKFZ-BT308 showed relative resistance to BCL-XLi. We therefore tested the dependence on BCL-XL protein in all four PA models in OIS. The number of viable cells relative to non-silencing control shRNA was reduced in all cell lines after BCL-XL knockdown with comparable efficiency (Supplementary Figure 4B and C), indicating a dependence on the protein for cell survival (Figure 4E), however without conclusive difference between the BCL-XLi resistant line and the sensitive lines (Figure 4E). Treatment with the two specific synthetic sensitizer BH3 peptides, BCL-2-antagonist of cell death (BAD; specific for dependence on BCL-2/BCL-XL) and activator of apoptosis harakiri (HRK; specific for dependence on BCL-XL) induced mitochondrial outer membrane permeabilization (MOMP) as measured by cytochrome c release to a similar extent in BCL-XLi sensitive (DKFZ-BT66) and resistant (DKFZ-BT308) cells (Figure 4F and G). In summary, target dependence and BCL-XL dependent priming were validated, however without differences to explain the low BCL-XLi sensitivity of DKFZ-BT308.

A Xenobiotics Metabolism Gene Set Upregulated in DKFZ-BT308 Predicts Navitoclax Resistance

We performed GSEA to discover potential differences between BCL-XL sensitive and resistant cell lines at mRNA level. 50 hallmark gene sets covering a wide range of biological

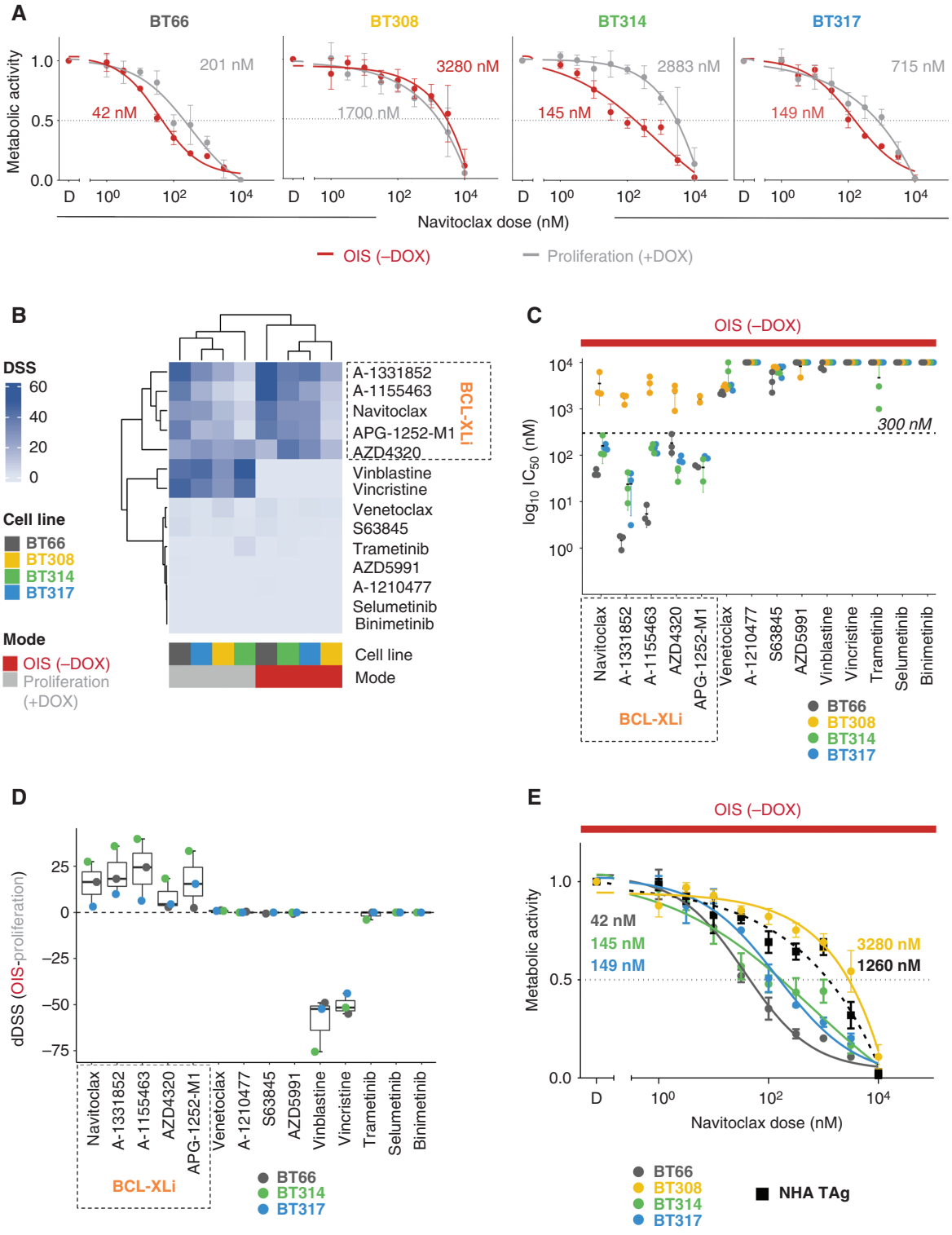

Fig. 2 Impact of BH3 mimetics on metabolic activity. (OIS (–DOX), oncogene-induced senescence, 5 days doxycycline withdrawal; proliferation (+DOX): +1 µg/ml doxycycline. D: DMSO; BCL-Xli: BCL-XL inhibitors). (A) Relative metabolic activity after treatment with navitoclax (ATP-based measurement of viable cells; mean ± SD of at least $n = 3$ biological replicates). (B) DSS (DSS3) of BH3 mimetics, chemotherapeutics, and MEKi in OIS and proliferation ($n = 3$ biological replicates for each drug, cell line, and mode). (C) Plot of log10 of absolute IC_{50} values of indicated drugs in OIS ($n = 3$ biological replicates ± SD). 10 µM (highest concentration applied) was assumed whenever insufficient drug effects precluded IC_{50} calculation. (D) Mean differential DSS (dDSS) of indicated drugs across three BCL-XLi sensitive PA cell lines (±SD). dDSS: DSS of cells in OIS – DSS of proliferating cells. (E) Relative metabolic activity (ATP-based measurement of viable cells) after treatment with navitoclax in normal human astrocytes NHA TAg compared to PA cell lines in OIS (mean ± SD; at least $n = 3$). Numbers in dose–response plots are absolute IC_{50}.

Table 1 Information on BH3 Mimetics

Compound	Inhibitory Profile (K_i Cell Free Assays; nM)				Approval/Clinical Trial Status in Adults	Example Clinical Trial	Achievable Non-toxic C_{max} (nM)	Reference (PMID)
	BCL-2	BCL-XL	BCL-W	MCL-1				
venetoclax	**<0.01**	48	245	>440	FDA approved *(CLL; SLL)*	n.a.	2533 ± 1612	23291630; 32171069
navitoclax	**<1**	**<0.05**	**<1**	550 (±40)	Phase 3	NCT02591095 *(ovarian cancer)*	6607 ± 3262	18451170; 21094089
AZD4320	3.9	4.5	n.a.	n.a.	Phase 1 *(dendrimer conjugate; AZD0466)*	NCT04214093 *(Hematologic or Solid Tumors)*	n.a.	32988967
APG-1252 (pelcitoclax)	**0.7**	**<1**	n.a.	n.a.	Phase 1/2	NCT03080311 NCT04210037 *(SCLC, other solid tumors)*	n.a.	24901320
AZD5991	n.a.	n.a.	n.a.	**0.7**	Phase 1/2	NCT03013998 *(AML)*	n.a.	30559424
A-1331852	6	**<0.01**	4	142	Preclinical	n.a.	n.a.	25787766
A-1155463	74	**<0.01**	8	>444	Preclinical	n.a.	n.a.	25787766
A-1210477	132	>660	2280	**<0.5**	Preclinical	n.a.	n.a.	25590800
S63845	>10000	>10000	n.a.	**<1.2**	Preclinical	n.a.	n.a.	27760111

n.a.: not available.
K_i values below 1.5 nM indicating strong target inhibition are marked in bold.

processes[38] were investigated in DKFZ-BT308 versus the BCL-XLi sensitive lines in OIS (Figure 5A). Among all gene sets, only the drug metabolism gene set "HALLMARK_XENOBIOTIC_METABOLISM" was significantly enriched in DKFZ-BT308 compared to the remaining cell lines (Figure 5B). Thirty eight genes of the gene set contributed to the core enrichment and were used to derive a new BT308_UP signature (Supplementary Table 4). To test a potential relation of this signature to BCL-XLi resistance, we used an independent data set of 751 cell lines (GDSC2)[26] (Figure 5C). GSEA and ssGSEA confirmed a significant enrichment of the BT308_UP signature in the group of navitoclax resistant cell lines (Figure 5D and E), as well as ABT-737 (another BCL-XLi) resistant cell lines (Supplementary Figure 5A). Binary logistic regression analysis revealed that expression of BT308_UP (independent continuous predictor) was able to predict "navitoclax resistance" at an optimal ssGSEA threshold score between –217 and –197 with $p = 3.37e^{-9}$, a sensitivity of 85.53%, and a specificity of 75.00% (Supplementary Figure 5B). Primary PAs showed a wide variability of BT308_UP signature expression, but all primary samples tested expressed the signature to a lower extent compared to the resistant cell line DKFZ-BT308 (Figure 5F). Taken together, we identified upregulation of a drug metabolism gene set in DKFZ-BT308 that could explain the phenotypical differences in BCL-XLi sensitivity.

Discussion

OIS is a well-known feature of PA[11,39] but currently not therapeutically exploited. The lack of preclinical data supporting senolytic drugs can be explained by the lack of PA OIS models. In this respect, the three new cell lines (DKFZ-BT308, DKFZ-BT314, and DKFZ-BT317) described in the present study are outstanding because they can be analyzed in OIS and complement the previously published DKFZ-BT66 model.

Using our four PA models, we discovered that BCL-XL is essential for PA cells in OIS and BH3 mimetics induce senolysis via inhibition of BCL-XL. Several recent studies have highlighted the potential role of senolysis in glioma therapy including BCL-XL inhibition.[40–42] However, these studies are fundamentally different from the pediatric low-grade glioma/OIS background of the present work since they investigated senolytics in another glioma type (adult high-grade glioma) and in the context of a different form of senescence (therapy-induced senescence). Beyond the first proof of BCL-XL as a target in PA, our study provides several translational implications. We confirmed abundance of the target BCL-XL in primary PA and higher expression of BCL-XL protein compared to normal CNS tissue. Of note, a broad variability in *BCL2L1*/BCL-XL expression among all primary samples was observed. However, this may not necessarily indicate differences in BCL-XLi susceptibility, as *BCL2L1* expression levels per se were not found to be predictive for dependence on BCL-XL in a recent study using different cancer cell lines.[43] Several BCL-XLi are already in clinical testing and therefore potentially available for studies in PA. Thrombocytopenia was a major dose-limiting toxicity observed in navitoclax phase I trials.[44,45] However, adjusted treatment schedules led to improved tolerability in adult patients[46] and two other BCL-Xli, AZD0466, and pelcitoclax, have shown lower platelet toxicity while maintaining anti-tumor activity.[47,48] The BCL-Xli responsive

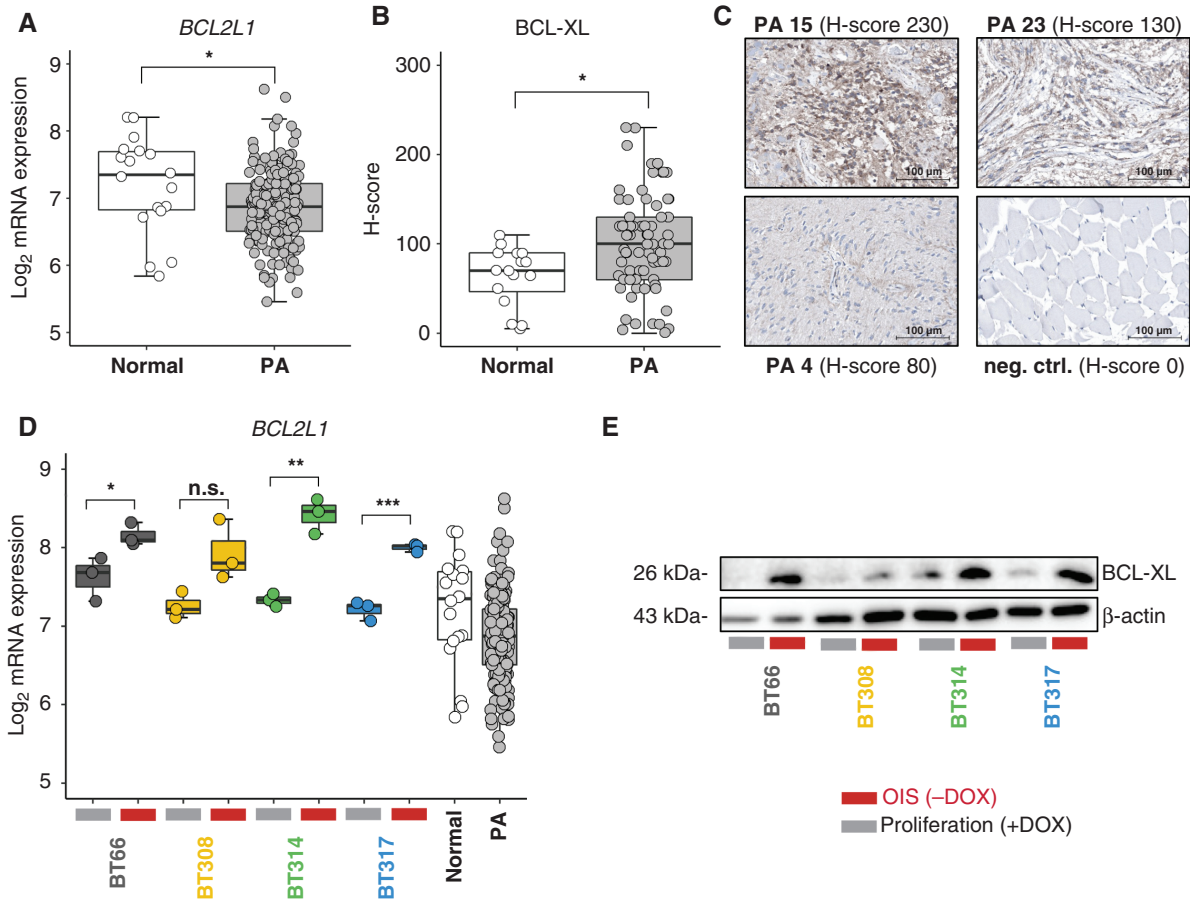

Fig. 3 BCL-XL expression in PA. (OIS (–DOX), oncogene-induced senescence, 5 days doxycycline withdrawal; proliferation (+DOX): +1 µg/ml doxycycline). (A) *BCL2L1* mRNA expression in primary PA compared to normal cerebellum. Expression data: ps_mkheidel_mkdkfz209_u133p2. Unpaired *t*-test: **P* < .05. (B) H-scores of BCL-XL protein staining intensity in 75 primary PA samples compared to 16 inconspicuous CNS tissues adjacent to low-grade gliomas. Unpaired t-test: **P* < .05. (C) Exemplary microscopic images of BCL-XL immunohistochemistry in PA showing strong (PA 15), medium (PA 23), and weak (PA 4) staining. neg. ctrl.: negative control, muscle tissue. Scale bars indicate a distance of 100 µm. (D) *BCL2L1* mRNA expression in four PA cell lines in proliferation vs. OIS compared to normal cerebellum (*n* = 18) and primary PA (*n* = 191) (ps_mkheidel_mkdkfz209_u133p2). Unpaired *t*-test: **P* < .05, ***P* < .01, ****P* < .001. (E) Western blot of BCL-XL protein in proliferation vs. OIS mode.

PA models were among the most navitoclax sensitive cell lines compared to cell lines from the GDSC2 database. The IC_{50} values of lower than 300 nM seem clinically relevant in the context of a navitoclax C_{max} of 6607 ± 3262 nM at RP2D.[44] No data is available on blood–brain barrier (BBB) penetrance of clinically available BCL-XLi. The relatively high molecular weight of navitoclax (974.61 g/mol), AZD4320 (954.5 g/mol) and pelcitoclax (1159.78 g/mol) might militate against an effective BBB penetrance per se. However, many PAs have a disrupted BBB, which is evident from the uptake of MR contrast agent in these tumors,[49,50] indicating that high molecular weights do not a priori preclude effective tumor concentrations of these compounds.

The BCL-XLi resistant cell line DKFZ-BT308 differed from the sensitive cell lines in expression of a xenobiotics and drug metabolism related gene set. This gene set was able to predict navitoclax resistance in an independent dataset, indicating that the genes differentially regulated in the resistant PA cell line are related to and involved in the observed resistance phenotype. Moreover, the BT308_UP signature was also enriched in cells resistant to the BH3 mimetic ABT-737, indicating an in-class relevance of this gene set. While resistance to BH3 mimetics has been linked to upregulation of non-inhibited BCL-2 members,[51] innate resistance caused by upregulation of drug metabolism genes has not been described in the context of BH3 mimetics so far and represents a new and possibly general observation that might be important also for many other cancer entities. A potential limitation of our observation is the lack of validation of this signature for the other BH3 mimetics used, as independent sensitivity data for these BH3 mimetics was not available. Expression of BT308_UP is variable within primary PA samples according to the presented data. Although the larger proportion of primary tumors shows an expression of the signature similar or lower compared to our sensitive cell lines, a smaller proportion showed higher expression of the BT308_UP signature, possibly indicative of relative resistance to BH3 mimetics. The clinical relevance and predictive

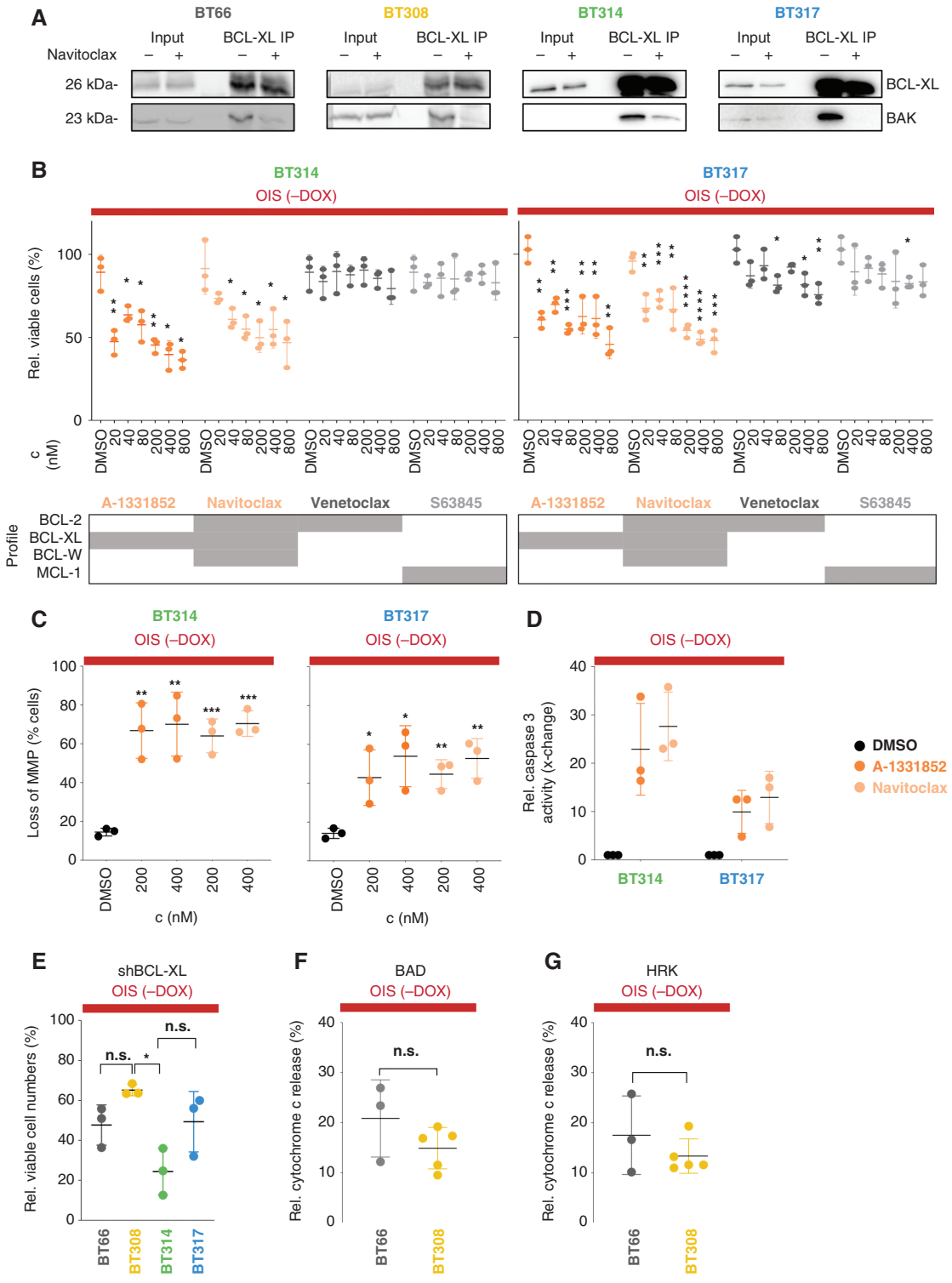

Fig. 4 On-target activity and cell death induction upon BCL-XLi treatment. (OIS (-DOX): oncogene-induced senescence; 5 days doxycycline withdrawal). (A) Western blot of BCL-XL and BAK after immunoprecipitation (IP) of BCL-XL after 4 h treatment of PA cells in OIS with 1 µM navitoclax. (B) Relative viable attached cells after 72 h of drug treatment (mean ± SD, $n = 3$ biological replicates). Grey boxes indicate drugs' inhibitory profiles ($K_i < 1$ nM). Unpaired *t*-test: $^*P < .05$, $^{**}P < .01$, $^{***}P < .001$. $^{****}P < .0001$ (comparison to DMSO). (C) Loss of mitochondrial membrane potential (MMP) measured by TMRE incorporation after 24 h treatment (mean ± SD, $n = 3$). Unpaired *t*-test. $^*P < .05$, $^{**}P < .01$, $^{***}P < .001$ (comparison to DMSO). (D) Relative caspase 3 activity after 24 h of treatment with 100 nM navitoclax or 100 nM A-1331852, control: DMSO (mean ± SD, n=3). (E) Relative viable cells 14 days after BCL-XL knock-down (100%: control shRNA) (mean ± SD, n=3). *Tukey multiple comparisons of means adjusted P-value < .01. (F, G) Relative cytochrome c released into the cytosol after 1 h of treatment with 10 µM BAD peptide (F) or 100 µM HRK peptide (G), respectively, relative to DMSO (mean ± SD, n = at least 3). rel.: relative; c: concentration.

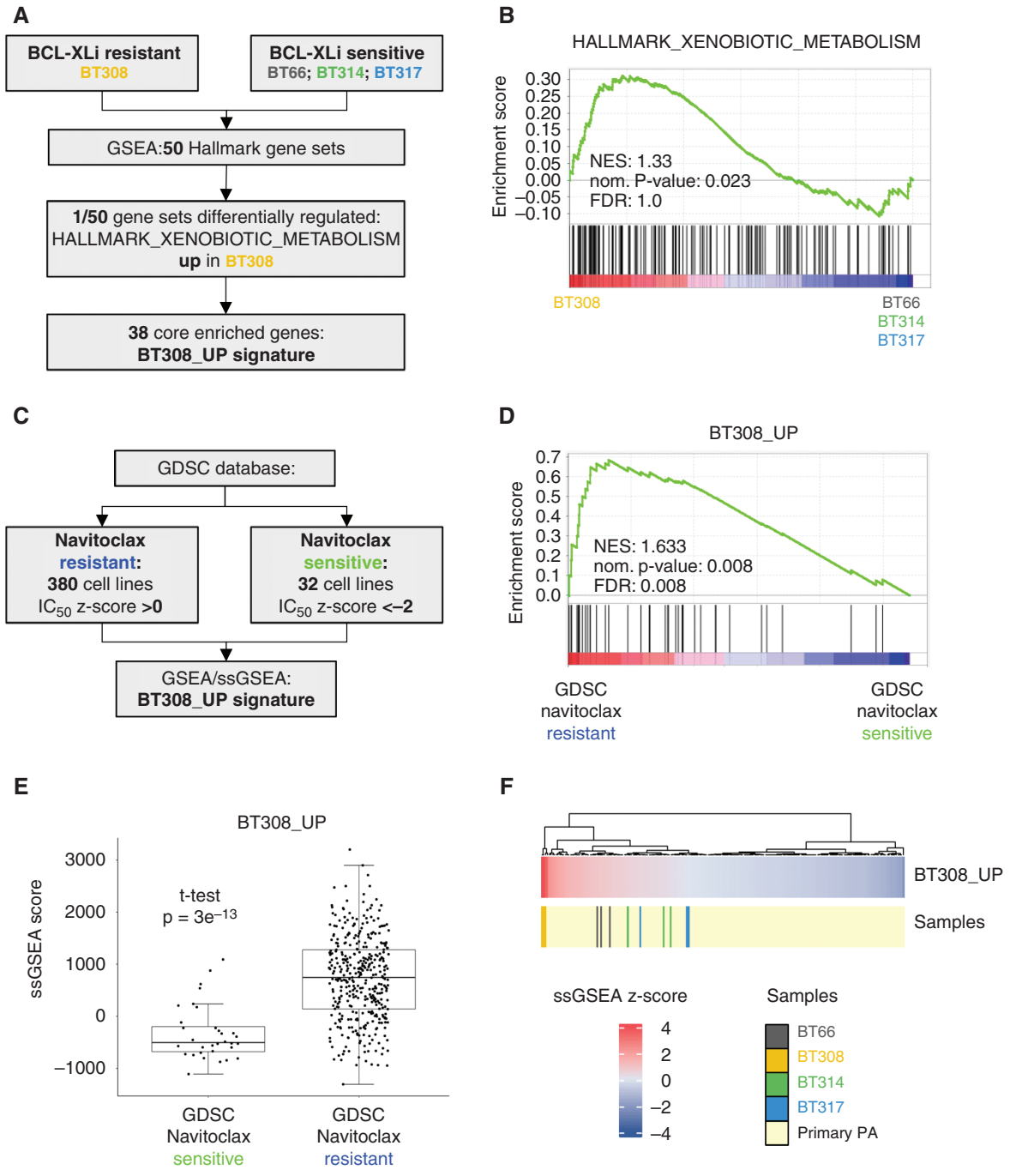

Fig. 5 Identification of a gene signature differentiating the BCL-XLi resistant cell line DKFZ-BT308 from BCL-XLi sensitive cell lines. (A) Flowchart depicting the deduction of BT308_UP signature. (B) GSEA of the HALLMARK_XENOBIOTIC_METABOLISM gene set in BT308 vs. BCL-Xli sensitive PA cell lines. (C) Work-flow of BT308_UP signature validation in the independent GDSC2 dataset. (D) Comparison of BT308_UP signature expression in the GDSC group "navitoclax resistant" vs. the GDSC group "navitoclax sensitive". (E) ssGSEA scores of BT308_UP signature in the two GDSC groups "navitoclax resistant" and "navitoclax sensitive". (F) BT308_UP signature ssGSEA z-scores in the four PA cell lines in OIS mode (n = 3 samples per cell line) and in primary PA (ps_mkheidel_mkdkfz209_u133p2). GSEA: geneset enrichment analysis; ssGSEA: single sample GSEA; NES: normalized enrichment score; norm.: normalized; FDR: false discovery rate.

validity of the signature described here needs to be prospectively validated in a clinical BCL-XLi trial.

In summary, our study provides the first reported target for senolytic treatment of PA cells. In contrast to chemotherapeutics and MEKi currently used in the treatment of PA, BCL-XLi induces apoptosis in PA cells in OIS. The main limitation of this study, as for most preclinical pLGG studies, is the lack of in vivo data. To our knowledge, there are no in vivo models of true molecular PA available to date that could be used for testing of

senolytic drugs in the context of OIS to surmount this obstacle. Based on the in vitro data presented here, BCL-XL inhibition is a promising treatment approach and the first attempt to target the so far un-targetable senescent compartment of PA tumors. The translation of our findings into clinical trials exploring the safety and efficacy of clinically available BCL-XLi in PA patients is urgently needed.

Supplementary Material

Supplementary material is available at *Neuro-Oncology* online.

Keywords

BCL-XL | BH3 mimetics | oncogene-induced senescence | pilocytic astrocytoma

Funding

The Brain Tumor Charity (TBTC, The Everest Centre for Low-Grade Pediatric Brain Tumours; GN-000382 to T.M., J.P.M.B., D.T.W.J., O.W. and S.M.P). DKTK German Cancer Consortium (DKTK JF Upgrade Next Gen LOGGIC; B310-JF-LOGGIC-MDE to T.M., O.W., D.C. and I.O.). Cancer Research UK (C54322/A27727 to J.P.M.B.). Ramon y Cajal Programme, Ministerio de Economia y Competitividad grant (RYC-2015-18357 to J.M.). Ministerio de Ciencia, Innovación y Universidades grant (RTI2018-094533-A-I00 to J.M.). P.B. was supported by the Pediatric Brain Tumor Foundation and the PLGA Program at Dana-Farber Cancer Institute. T.M. was supported by the Bilger family.

Acknowledgments

We thank the patients and families for consent to collect and use tumor material. We thank Daniela Kuhn, Isabel Büdenbender, Carina Müller and Anna Laudat for excellent technical support. J.P.M.B. is grateful to the Great Ormond Street Hospital Charity and NIHR Biomedical Research Centre at University College London Hospitals NHS Foundation Trust and University College London. We thank the Microarray Unit of the Genomics and Proteomics Core Facility, DKFZ, for providing excellent Expression Profiling services.

Conflict of interest statement. T.M. received research funding from Biomed Valley and Day One Therapeutics. C.M.T. participated in advisory boards of Novartis and Bayer. S.M.P. receives funding from Bayer, Pfizer, Eli-Lilly, Roche, Amgen, Astra Zeneca, PharmaMar, Sanofi and Servier in the context of an IMI-2-funded EU project entitled ITCC-P4 (www.itccp4.eu). O.W. participated in advisory boards of Novartis, BMS, Janssen and receives research grants from BVD, Day One Therapeutics. J.D. and Y.Z. are employees of Ascentage Pharma. J.M. is co-inventor of dynamic BH3 profiling, was paid consultant for Oncoheroes Biosciences and Vivid Biosciences, is unpaid board member for The Society for Functional Precision Medicine, is collaborating with AstraZeneca.

Authorship statement. Conceptualization: F.Se., T.M., O.W.; data generation: F.Se., R.S., G.V., P.S., J.Z., R.G., C.A., J.W.T., S.S. F.Sa.; Data analysis: F.Se., R.S., G.V., P.S., J.Z., C.A., H.P., J.W.T., R.G., S.S., J.P.M.B., S.P., P.B., S.M.P., J.M., D.C., I.O., F.Sa., D.T.W.J.; Writing of original draft: F.Se. and T.M.; Acquisition of patient samples and relevant clinical data: F.Se., C.M.T., M.U.S., A.E.D., C.H.-M., J.W.T., P.B., D.C., D.T.W.J.; Writing, review, and editing: all authors; Supervision: T.M.

References

1. Ostrom QT, de Blank PM, Kruchko C, et al. Alex's lemonade stand foundation infant and childhood primary brain and central nervous system tumors diagnosed in the United States in 2007-2011. *Neuro Oncol.* 2015; 16(Suppl 10):x1–x36.
2. Gnekow AK, Falkenstein F, von Hornstein S, et al. Long-term follow-up of the multicenter, multidisciplinary treatment study HIT-LGG-1996 for low-grade glioma in children and adolescents of the German speaking society of pediatric oncology and hematology. *Neuro Oncol.* 2012; 14(10):1265–1284.
3. Jones DT, Kocialkowski S, Liu L, et al. Tandem duplication producing a novel oncogenic BRAF fusion gene defines the majority of pilocytic astrocytomas. *Cancer Res.* 2008; 68(21):8673–8677.
4. Jones DT, Hutter B, Jager N, et al. Recurrent somatic alterations of FGFR1 and NTRK2 in pilocytic astrocytoma. *Nat Genet.* 2013; 45(8):927–932.
5. Selt F, van Tilburg CM, Bison B, et al. Response to trametinib treatment in progressive pediatric low-grade glioma patients. *J Neurooncol.* 2020; 149(3):499–510.
6. Manoharan N, Choi J, Chordas C, et al. Trametinib for the treatment of recurrent/progressive pediatric low-grade glioma. *J Neurooncol.* 2020; 149(2):253–262.
7. Kondyli M, Larouche V, Saint-Martin C, et al. Trametinib for progressive pediatric low-grade gliomas. *J Neurooncol.* 2018; 140(2):435–444.
8. Fangusaro J, Onar-Thomas A, Young Poussaint T, et al. Selumetinib in paediatric patients with BRAF-aberrant or neurofibromatosis type 1-associated recurrent, refractory, or progressive low-grade glioma: a multicentre, phase 2 trial. *Lancet Oncol.* 2019; 20(7):1011–1022.
9. Banerjee A, Jakacki RI, Onar-Thomas A, et al. A phase I trial of the MEK inhibitor selumetinib (AZD6244) in pediatric patients with recurrent or refractory low-grade glioma: a Pediatric Brain Tumor Consortium (PBTC) study. *Neuro-Oncology.* 2017; 19(8):1135–1144.
10. Knight T, Shatara M, Carvalho L, et al. Dramatic response to trametinib in a male child with neurofibromatosis type 1 and refractory astrocytoma. *Pediatric Blood Cancer.* 2019; 66(1):e27474.
11. Jacob K, Quang-Khuong DA, Jones DT, et al. Genetic aberrations leading to MAPK pathway activation mediate oncogene-induced senescence in sporadic pilocytic astrocytomas. *Clin Cancer Res.* 2011; 17(14):4650–4660.
12. Sengupta S, Chatterjee U, Banerjee U, et al. A study of histopathological spectrum and expression of Ki-67, TP53 in primary brain tumors of pediatric age group. *Indian J Med Paediatr Oncol.* 2012; 33(1):25–31.
13. Carreno G, Guiho R, Martinez-Barbera JP. Cell senescence in neuropathology: a focus on neurodegeneration and tumours. *Neuropathol Appl Neurobiol.* 2021; 47(3):359–378.

14. Zhu Y, Tchkonia T, Pirtskhalava T, et al. The Achilles' heel of senescent cells: from transcriptome to senolytic drugs. *Aging Cell.* 2015; 14(4):644–658.
15. Zhu Y, Tchkonia T, Fuhrmann-Stroissnigg H, et al. Identification of a novel senolytic agent, navitoclax, targeting the Bcl-2 family of anti-apoptotic factors. *Aging Cell.* 2016; 15(3):428–435.
16. Zhu Y, Doornebal EJ, Pirtskhalava T, et al. New agents that target senescent cells: the flavone, fisetin, and the BCL-XL inhibitors, A1331852 and A1155463. *Aging (Albany NY).* 2017; 9(3):955–963.
17. Yosef R, Pilpel N, Tokarsky-Amiel R, et al. Directed elimination of senescent cells by inhibition of BCL-W and BCL-XL. *Nat Commun.* 2016; 7:11190.
18. Chang J, Wang Y, Shao L, et al. Clearance of senescent cells by ABT263 rejuvenates aged hematopoietic stem cells in mice. *Nat Med.* 2016; 22(1):78–83.
19. Kale J, Osterlund EJ, Andrews DW. BCL-2 family proteins: changing partners in the dance towards death. *Cell Death Differ.* 2018; 25(1):65–80.
20. Buhl JL, Selt F, Hielscher T, et al. The senescence-associated secretory phenotype mediates oncogene-induced senescence in pediatric pilocytic astrocytoma. *Clin Cancer Res.* 2019; 25(6):1851–1866.
21. Bid HK, Kibler A, Phelps DA, et al. Development, characterization, and reversal of acquired resistance to the MEK1 inhibitor selumetinib (AZD6244) in an in vivo model of childhood astrocytoma. *Clin Cancer Res.* 2013; 19(24):6716–6729.
22. Yuan M, White D, Resar L, et al. Conditional reprogramming culture conditions facilitate growth of lower-grade glioma models. *Neuro Oncol.* 2021; 23(5):770–782.
23. Bax DA, Little SE, Gaspar N, et al. Molecular and phenotypic characterisation of paediatric glioma cell lines as models for preclinical drug development. *PLoS One.* 2009; 4(4):e5209.
24. Selt F, Hohloch J, Hielscher T, et al. Establishment and application of a novel patient-derived KIAA1549:BRAF-driven pediatric pilocytic astrocytoma model for preclinical drug testing. *Oncotarget.* 2017; 8(7):11460–11479.
25. Yadav B, Pemovska T, Szwajda A, et al. Quantitative scoring of differential drug sensitivity for individually optimized anticancer therapies. *Sci Rep.* 2014; 4:5193.
26. Yang W, Soares J, Greninger P, et al. Genomics of Drug Sensitivity in Cancer (GDSC): a resource for therapeutic biomarker discovery in cancer cells. *Nucleic Acids Res.* 2013; 41(Database issue):D955–D961.
27. Mootha VK, Lindgren CM, Eriksson KF, et al. PGC-1alpha-responsive genes involved in oxidative phosphorylation are coordinately downregulated in human diabetes. *Nat Genet.* 2003; 34(3):267–273.
28. Subramanian A, Tamayo P, Mootha VK, et al. Gene set enrichment analysis: a knowledge-based approach for interpreting genome-wide expression profiles. *Proc Natl Acad Sci USA.* 2005; 102(43):15545–15550.
29. Barbie DA, Tamayo P, Boehm JS, et al. Systematic RNA interference reveals that oncogenic KRAS-driven cancers require TBK1. *Nature.* 2009; 462(7269):108–112.
30. Reich M, Liefeld T, Gould J, et al. GenePattern 2.0. *Nat Genet.* 2006; 38(5):500–501.
31. Reitman ZJ, Paolella BR, Bergthold G, et al. Mitogenic and progenitor gene programmes in single pilocytic astrocytoma cells. *Nat Commun.* 2019; 10(1):3731.
32. Sahm F, Schrimpf D, Jones DT, et al. Next-generation sequencing in routine brain tumor diagnostics enables an integrated diagnosis and identifies actionable targets. *Acta Neuropathol.* 2016; 131(6):903–910.
33. Capper D, Jones DTW, Sill M, et al. DNA methylation-based classification of central nervous system tumours. *Nature.* 2018; 555(7697):469–474.
34. Ryan J, Montero J, Rocco J, Letai A. iBH3: simple, fixable BH3 profiling to determine apoptotic priming in primary tissue by flow cytometry. *Biol Chem.* 2016; 397(7):671–678.
35. Capper D, Stichel D, Sahm F, et al. Practical implementation of DNA methylation and copy-number-based CNS tumor diagnostics: the Heidelberg experience. *Acta Neuropathol.* 2018; 136(2):181–210.
36. Wagle MC, Kirouac D, Klijn C, et al. A transcriptional MAPK Pathway Activity Score (MPAS) is a clinically relevant biomarker in multiple cancer types. *NPJ Precis Oncol.* 2018; 2(1):7.
37. Fridman AL, Tainsky MA. Critical pathways in cellular senescence and immortalization revealed by gene expression profiling. *Oncogene.* 2008; 27(46):5975–5987.
38. Liberzon A, Birger C, Thorvaldsdottir H, et al. The Molecular Signatures Database (MSigDB) hallmark gene set collection. *Cell Syst.* 2015; 1(6):417–425.
39. Raabe EH, Lim KS, Kim JM, et al. BRAF activation induces transformation and then senescence in human neural stem cells: a pilocytic astrocytoma model. *Clin Cancer Res.* 2011; 17(11):3590–3599.
40. Schwarzenbach C, Tatsch L, Brandstetter Vilar J, et al. Targeting c-IAP1, c-IAP2, and Bcl-2 eliminates senescent glioblastoma cells following temozolomide treatment. *Cancers (Basel).* 2021; 13(14):3585.
41. Rahman M, Olson I, Mansour M, et al. Selective vulnerability of senescent glioblastoma cells to BCL-XL inhibition. *Mol Cancer Res.* 2022; 20(6):938–948.
42. Fletcher-Sananikone E, Kanji S, Tomimatsu N, et al. Elimination of radiation-induced senescence in the brain tumor microenvironment attenuates glioblastoma recurrence. *Cancer Res.* 2021; 81(23):5935–5947.
43. Soderquist RS, Crawford L, Liu E, et al. Systematic mapping of BCL-2 gene dependencies in cancer reveals molecular determinants of BH3 mimetic sensitivity. *Nat Commun.* 2018; 9(1):3513.
44. Wilson WH, O'Connor OA, Czuczman MS, et al. Navitoclax, a targeted high-affinity inhibitor of BCL-2, in lymphoid malignancies: a phase 1 dose-escalation study of safety, pharmacokinetics, pharmacodynamics, and antitumour activity. *Lancet Oncol.* 2010; 11(12):1149–1159.
45. Cleary JM, Lima CM, Hurwitz HI, et al. A phase I clinical trial of navitoclax, a targeted high-affinity Bcl-2 family inhibitor, in combination with gemcitabine in patients with solid tumors. *Invest New Drugs.* 2014; 32(5):937–945.
46. de Vos S, Leonard JP, Friedberg JW, et al. Safety and efficacy of navitoclax, a BCL-2 and BCL-XL inhibitor, in patients with relapsed or refractory lymphoid malignancies: results from a phase 2a study. *Leuk Lymphoma.* 2021; 62(4):810–818.
47. Nehal J, Lakhani DWR, Qi Z, et al. First-in-human study of palcitoclax (APG-1252), a novel dual Bcl-2/Bcl-xL inhibitor, demonstrated advantages in platelet safety while maintaining anticancer effect in U.S. patients with metastatic solid tumors. *J Clin Oncol.* 2020; 38(15_suppl).
48. Balachander SB, Criscione SW, Byth KF, et al. AZD4320, a dual inhibitor of Bcl-2 and Bcl-xL, induces tumor regression in hematologic cancer models without dose-limiting thrombocytopenia. *Clin Cancer Res.* 2020; 26(24):6535–6549.
49. Sievert AJ, Fisher MJ. Pediatric low-grade gliomas. *J Child Neurol.* 2009; 24(11):1397–1408.
50. Fangusaro J, Witt O, Hernaiz Driever P, et al. Response assessment in paediatric low-grade glioma: recommendations from the Response Assessment in Pediatric Neuro-Oncology (RAPNO) working group. *Lancet Oncol.* 2020; 21(6):e305–e316.
51. Stamelos VA, Redman CW, Richardson A. Understanding sensitivity to BH3 mimetics: ABT-737 as a case study to foresee the complexities of personalized medicine. *J Mol Signal.* 2012; 7(1):12.